

Magnetically Active Stars in Taurus–Auriga: Photometric Variability and Basic Physical Parameters

K. N. Grankin

Crimean Astrophysical Observatory, Nauchny, Crimea, 98409 Ukraine

konstantin.grankin@rambler.ru

Abstract

The paper presents an analysis of homogeneous long-term photometric observations of 28 well-known weak-line T Tauri stars (WTTS) and 60 WTTS candidates detected by the ROSAT observatory in the direction of the Taurus–Auriga star-forming region. 22 known WTTS and 39 WTTS candidates are shown to exhibit periodic light variations that are attributable to the phenomenon of spotted rotational modulation. The rotation periods of these spotted stars lie within the range from 0.5 to 10 days. Significant differences between the long-term photometric behaviors of known WTTS and WTTS candidates have been found. We have calculated accurate luminosities, radii, masses, and ages for 74 stars. About 33% of the sample of WTTS candidates have ages younger than 10 Myr. The mean distance to 24 WTTS candidates with reliable estimates of their radii is shown to be 143 ± 26 pc. This is in excellent agreement with the adopted distance to the Taurus–Auriga star-forming region.

Key words: *stars – variable, properties, rotation, pre-main-sequence stars.*

INTRODUCTION

The all-sky survey with the ROSAT X-ray space observatory has revealed a large number of magnetically active late-type stars in the neighborhoods of star-forming regions. In particular, Wichmann et al. (1996) identified 76 candidates for T Tauri stars (TTS) toward the Taurus–Auriga star-forming region (SFR). Subsequently, Wichmann et al. (2000) undertook a detailed study of 58 TTS candidates based on high-resolution echelle spectroscopy and proper motions. They found that about 60% of this sample could be regarded as pre-main-sequence (PMS) stars, while the remaining stars are probably zero-age main-sequence (ZAMS) stars.

Bouvier et al. (1997) undertook the first photometric monitoring of 58 stars from Wichmann’s list to measure their rotation periods. They found the photometric periods for 18 stars. Subsequently, Broeg et al. (2006) investigated 10 spectroscopic binaries from Wichmann’s list. They confirmed the periods for four stars and were the first to detect periodicities for six objects. Concurrently, Xing et al. (2006) reported the detection of periods for three more stars.

Owing to these works, the number of stars from Wichmann’s list with known rotation periods increased to 27. Grankin et al. (2007a) undertook a long-term photometric study of 39 objects from Wichmann’s list during several observing seasons and were able to find periodic light variations for 22 stars for the first time. This result allowed the number of stars from Wichmann’s list with known periods to be almost doubled.

Thus, on the one hand, there are long-term photometric measurements for 28 young stars in the Taurus–Auriga SFR with a known evolutionary status (see Grankin et al. 2008); 22 stars from this group exhibit periodic light variations (below, they will be mentioned as well-known WTTS or stars from Grankin’s list). On the other hand, there are such data for 60 magnetically active stars with a controversial evolutionary status (WTTS candidates or stars from Wichmann’s list); 39 stars from this second group exhibit periodic light variations (see Grankin et al. 2007a).

In this paper, we use homogeneous long-term photometry for 28 well-known WTTS from Grankin’s list and 60 WTTS candidates from Wichmann’s list to determine their basic physical parameters and to improve the data on these magnetically active stars in the Taurus–Auriga SFR.

OBSERVATIONS

All our broadband BVR observations for the stars from Wichmann’s list were obtained at the Maidanak Astronomical Observatory (longitude $E4^{\text{h}}27^{\text{m}}47^{\text{s}}$; latitude $+38^{\circ}41'$; altitude 2709 m). For our long-term monitoring, we selected 62 stars with $V < 14.^{\text{m}}4$. More than 5000 BVR magnitudes were obtained for these objects in the period between 1994 and 2006. All our observations were performed with three telescopes (one 0.48-m and two 0.6-m reflectors) using identical single-channel pulse-counting photometers with FEU-79 photomultiplier tubes. A detailed description of the observing and data reduction technique can be found in Grankin et al. (2008).

The results of the Maidanak program of homogeneous long-term photometry for 62 WTTS candidates from Wichmann’s list are presented in Table 1. The columns in Table 1 give: the star number in Wichmann’s list, the star name, the epoch of observations, the number of observing seasons (N_s), the number of observations in the V band (N_{obs}), the mean brightness level ($\overline{V_m}$) and its seasonal standard deviation (σ_{V_m}), the mean photometric amplitude ($\overline{\Delta V}$, averaged over all seasons) and its seasonal standard deviation ($\sigma_{\Delta V}$), and the mean colors $\overline{B-V}$ and $\overline{V-R}$. The series of statistical parameters given in the last six columns was determined and discussed in detail previously (see Grankin et al. 2007b, 2008).

BASIC PHOTOMETRIC PROPERTIES

The stars of our sample exhibit a low variability level. Analysis of the mean variability amplitude distribution (histogram) in the V band for 60 WTTS candidates from Wichmann’s list showed that it is sharp-pointed, with $\overline{\Delta V}$ in the range from $0.^{\text{m}}05$ to $0.^{\text{m}}30$. Indeed, most of the stars in this sample exhibit small variability amplitudes (between $0.^{\text{m}}05$ and $0.^{\text{m}}15$) and only two stars (3%) have mean amplitudes in the V band larger than $0.^{\text{m}}2$. The maximum of the distribution lies near $0.^{\text{m}}1$. Here and below, we excluded two stars (N9 and N72) from our analysis, because their photometric variability was not caused by rotational modulation. More detailed information about these two stars will be given in the section devoted to the results of our periodogram analysis.

The mean brightness level of the stars seems very stable during long-term observations, with a very small standard deviation σ_{V_m} . Most of the stars (85%) show $\sigma_{V_m} \leq 0.^m06$. The remaining stars exhibit σ_{V_m} between $0.^m08$ and $0.^m12$. Likewise, the changes in the photometric amplitude from season to season characterized by $\sigma_{\Delta V}$ are small and do not exceed $0.^m06$.

PERIODOGRAM ANALYSIS

We used three different methods to find the rotation periods: the χ^2 technique, the “string-length” algorithm, and the Lomb–Scargle periodogram analysis (for more detailed information, see Grankin et al. 2008). The existence of spurious periods is the main problem that we faced when searching for periodic light variations. As a rule, we observed each object once in a night over 1–2 months during each season. Such a distribution of observations in time gives rise to the so-called spurious periods (Tanner 1948). Both true and spurious periods produce exactly equivalent (in the statistical sense) folded light curves. Two or three magnitude estimates should be obtained during one night to determine the true period. Such intense observations were performed for 42 stars from Wichmann’s list. For each selected star, we made two or three *BVR* measurements during each night. The availability of several short-term monitorings allowed us to calculate the rate of change in the brightness of a star ($\Delta V/\Delta t$) and to find the true periodicity among the whole set of spurious periods. In addition, such an observing technique revealed short periods ($P < 1$ days).

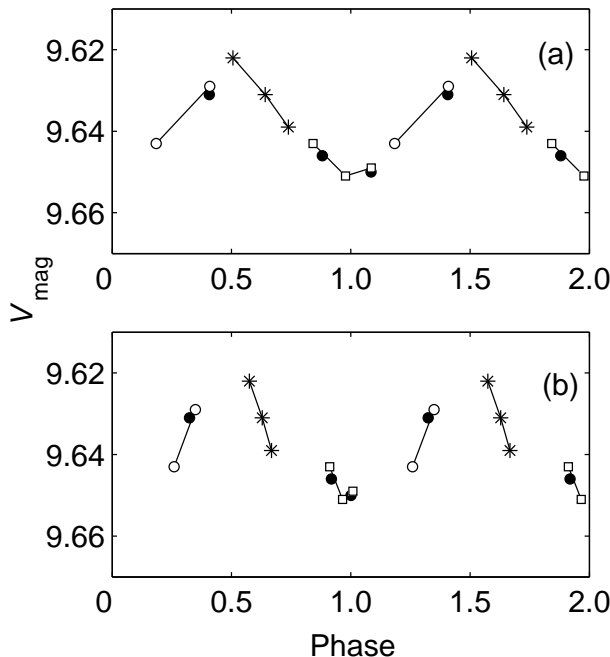


Figure 1: Phase light curve for RX J0441.8+2658 (number 50 in Wichmann’s list) for two different periods: (a) $P = 0.600$ days and (b) $P = 1.506$ days. The monitoring observations during each individual night in 2006 are designated by identical symbols and are connected by the solid line. The isolated observations are marked by the black circles.

Figure 1 presents an example of the phase light curves for star N50 from Wichmann’s list. We found two most probable periods for this star in the 2003 observations: 0.600 (Fig. 1a) and 1.506 days (Fig. 1b). One of them is true and the other is spurious. Owing to the monitoring observations performed in 2006, we were able to show that the shorter period is true.

Table 1: Long-term photometry for WTTS candidates from Wichmann’s list (Wichmann et al. 1996)

W96	Name	Epoch	N_s	N_{obs}	\overline{V}_m	σ_{V_m}	$\overline{\Delta V}$	$\sigma_{\Delta V}$	$\overline{B-V}$	$\overline{V-R}$
1	RX J0400.5+1935	1995-2005	4	103	10.19	0.014	0.12	0.036	0.94	0.82
2	RX J0403.3+1725	1995-2005	4	75	11.70	0.012	0.12	0.049	1.10	0.95
3	RX J0405.1+2632	1999-2005	6	121	11.35	0.062	0.09	0.019	0.86	0.74
4	RX J0405.3+2009	1995-2005	4	95	10.41	0.033	0.11	0.037	0.91	0.77
5	RX J0405.7+2248	1994-2006	5	109	9.36	0.038	0.05	0.008	0.63	0.58
6	RX J0406.7+2018	1994-2006	5	94	9.65	0.084	0.05	0.018	0.58	0.53
7	RX J0406.8+2541	2004-2006	3	53	11.91	0.048	0.30	0.029	1.38	1.28
8	RX J0407.8+1750	1994-2005	4	61	11.46	0.091	0.07	0.027	0.86	0.80
9	RX J0408.2+1956	1994-2005	3	61	13.00	0.063	0.41	0.266	1.28	1.11
10	RX J0409.1+2901	1994-2005	11	259	10.56	0.018	0.10	0.029	0.84	0.75
11	RX J0409.2+1716	2003-2005	3	32	13.30	0.009	0.09	0.025	1.40	1.43
12	RX J0409.8+2446	2003-2005	3	43	13.48	0.007	0.16	0.061	1.47	1.48
13	RX J0412.8+1937	1995-2005	4	76	12.57	0.029	0.09	0.010	1.30	1.18
14	RX J0412.8+2442	1995-2005	4	74	12.00	0.020	0.08	0.023	1.07	1.01
15	RX J0413.0+1612	1994-2006	5	95	11.02	0.074	0.04	0.015	0.74	0.66
18	RX J0415.3+2044	1994-2005	11	224	10.65	0.031	0.10	0.044	0.72	0.66
19	RX J0415.8+3100	1995-2005	4	102	12.36	0.057	0.10	0.023	0.89	0.82
23	RX J0420.3+3123	2004-2006	3	62	12.56	0.022	0.16	0.019	1.08	0.96
27	RX J0423.7+1537	1994-2005	11	225	11.25	0.026	0.10	0.017	0.93	0.81
29	RX J0424.8+2643B	1999-2005	6	89	11.34	0.049	0.10	0.021	1.32	1.20
28	RX J0424.8+2643A	1999-2005	6	83	11.42	0.045	0.06	0.011	1.35	1.23
30	RX J0427.1+1812	1999-2005	6	100	9.42	0.044	0.07	0.034	0.56	0.53
31	RX J0430.8+2113	1995-2005	4	97	10.34	0.007	0.11	0.023	0.72	0.65
32	RX J0431.3+2150	1994-2005	11	223	10.81	0.037	0.10	0.027	0.83	0.71
36	RX J0432.7+1853	1994-2005	4	68	10.81	0.020	0.09	0.044	0.82	0.70
37	RX J0432.8+1735	2004-2005	2	28	13.71	0.046	0.08	0.023	1.65	1.59
38	RX J0433.5+1916	2003-2005	3	52	13.13	0.011	0.09	0.009	1.03	0.92
39	RX J0433.7+1823	2003-2005	3	35	12.07	0.019	0.05	0.008	1.06	0.95
40	RX J0435.9+2352	2004-2005	2	33	13.41	0.029	0.15	0.017	1.55	1.58
41	RX J0437.2+3108	2003-2005	3	30	13.23	0.058	0.08	0.006	1.34	1.25
44	RX J0438.2+2023	1994-2006	5	76	12.20	0.008	0.10	0.037	1.12	0.97
45	RX J0438.2+2302	2004-2005	2	31	13.83	0.011	0.09	0.007	1.48	1.40
46	RX J0438.4+1543	1995-2005	4	64	13.34	0.105	0.09	0.012	1.21	1.09
47	RX J0438.7+1546	1994-2005	4	51	10.83	0.074	0.10	0.048	0.99	0.87
48	RX J0439.4+3332A	1994-2006	5	85	11.48	0.030	0.11	0.050	1.19	1.06
49	RX J0441.4+2715	2003-2005	3	25	13.10	0.042	0.04	0.012	0.98	0.92
50	RX J0441.8+2658	1994-2006	5	61	9.59	0.088	0.04	0.009	0.60	0.58
51	RX J0443.4+1546	1999-2005	6	68	12.88	0.037	0.08	0.040	1.03	0.95
52	RX J0444.3+2017	1994-2005	4	54	12.64	0.048	0.12	0.016	1.14	1.02
53	RX J0444.4+1952	1994-2005	4	53	12.57	0.017	0.09	0.033	1.49	1.41
54	RX J0444.9+2717	1994-2005	4	49	9.59	0.115	0.06	0.013	0.91	0.82
55	RX J0445.8+1556	1994-2005	4	63	9.35	0.045	0.11	0.039	0.75	0.67
56	RX J0446.8+2255	2003-2005	3	36	12.88	0.023	0.13	0.016	1.43	1.38
57	RX J0447.9+2755	1999-2005	6	86	12.41	0.041	0.10	0.020	1.12	1.02
58	RX J0450.0+2230	1995-2005	4	77	11.22	0.023	0.11	0.030	0.89	0.78

Table 1: continued.

W96	Name	Epoch	N_s	N_{obs}	\overline{V}_m	σ_{V_m}	$\overline{\Delta V}$	$\sigma_{\Delta V}$	$\overline{B-V}$	$\overline{V-R}$
59	RX J0451.8+1758	2004-2005	2	22	14.02	0.028	0.14	0.062	1.56	1.59
60	RX J0451.9+2849A	2004-2005	2	22	13.36	0.061	0.14	0.072	1.30	1.15
61	RX J0451.9+2849B	2004-2005	2	22	14.13	0.013	0.10	0.018	1.15	1.02
62	RX J0452.5+1730	1999-2005	6	83	12.06	0.023	0.06	0.025	1.09	0.95
63	RX J0452.8+1621	1999-2005	6	94	11.69	0.015	0.11	0.024	1.30	1.15
64	RX J0452.9+1920	1999-2005	6	90	12.16	0.083	0.06	0.024	1.09	0.99
65	RX J0453.1+3311	2004-2005	2	24	13.80	0.052	0.10	0.051	1.07	0.93
66	RX J0455.2+1826	1994-2005	4	70	9.22	0.016	0.05	0.016	0.62	0.57
67	RX J0455.7+1742	1999-2005	6	100	11.21	0.015	0.08	0.019	1.02	0.89
68	RX J0456.2+1554	2003-2005	3	39	12.67	0.024	0.11	0.049	1.31	1.17
70	RX J0457.0+1600	2004-2005	2	22	14.35	0.023	0.22	0.045	1.54	1.52
71	RX J0457.0+1517	1994-2006	5	81	10.30	0.013	0.05	0.018	0.66	0.61
72	RX J0457.0+3142	1994-2005	11	261	10.63	0.044	0.14	0.065	1.62	1.35
73	RX J0457.2+1524	1994-2006	5	78	10.25	0.034	0.08	0.020	0.96	0.83
74	RX J0457.5+2014	1994-2005	4	67	11.06	0.051	0.11	0.035	0.87	0.78
75	RX J0458.7+2046	1994-2006	12	210	11.92	0.026	0.09	0.026	1.24	1.08
76	RX J0459.7+1430	1999-2006	7	108	11.71	0.048	0.14	0.074	1.07	0.96

To reveal the true periods for the stars without monitoring observations, we used a statistical method based on Monte Carlo simulations (A. Nemec and J. Nemec 1985). To guarantee a reliable significance level, we established a minimum number of permutations equal to 1000. The periods were searched for in the interval from 0.5 to 20 days. If the false alarm probability was between 0.00 and 0.01, then the period was considered true with a 95% confidence.

RESULTS OF OUR PERIODOGRAM ANALYSIS

As a result of the periodogram analysis of our long-term observations for the stars from Wichmann's list, periodic light variations were detected for the first time in 22 stars and their periods were improved for 19 more objects. Preliminary data on the rotation periods of 22 stars can be found in Grankin et al. (2007a). Table 2 presents information only about those 19 objects for which the previously published rotation periods were confirmed or improved. The columns in Table 2 present the star number in Wichmann's list, the star name, the minimum and maximum amplitudes of periodic light variations (ΔV_{min} and ΔV_{max}), and the period.

Two stars show periodic light variations that are not produced by spotted rotational modulation. As is already well known, the first star, RX J0408.2+1956, is an eclipsing binary with a period of 3.01 days (see Bouvier et al. 1997; Broeg et al. 2006). Four observing seasons allowed the period to be improved. It is limited by $P = 3.0093 \pm 0.0001$ days. The heliocentric epoch of minimum is $HJD_{\text{min}} = 2449658.40$. The second star, RX J0457.0+3142, is also known as V501 Aur. Its photometric period is close to 56 days and this is most likely not the rotation period (see Grankin et al. 2008). We will disregard these two objects, because we are planning to discuss the periods attributable only to rotational modulation.

Table 2: WTTS candidates with confirmed or improved periods

W96	Name	ΔV_{\min}	ΔV_{\max}	P (days)				
				this paper	bo97	br06	xi06	gr08
2	RX J0403.3+1725	0.08	0.11	0.573	0.573	0.574	0.287	
7	RX J0406.8+2541	0.28	0.33	1.6906	1.73	1.70		
9	RX J0408.2+1956	0.18	0.70	3.0093	3.02	3.0109		
10	RX J0409.1+2901	0.06	0.16	2.662	2.74:			2.662
11	RX J0409.2+1716	0.07	0.09	0.613		0.60		
14	RX J0412.8+2442	0.05	0.11	0.865	6.7			
18	RX J0415.3+2044	0.06	0.21	1.8122	1.83			1.8122
23	RX J0420.3+3123	0.14	0.17	4.429	4.2			
27	RX J0423.7+1537	0.08	0.13	1.605	1.605			1.605
32	RX J0431.3+2150	0.06	0.19	2.7136	2.71			2.7136
36	RX J0432.7+1853	0.06	0.13	1.561	1.55		1.558	
47	RX J0438.7+1546	0.10	0.14	3.0789	3.07			
52	RX J0444.3+2017	0.11	0.14	1.1320	1.15			
55	RX J0445.8+1556	0.04	0.15	1.1040	1.104			
63	RX J0452.8+1621	0.09	0.16	3.46		3.6		
71	RX J0457.0+1517	0.03	0.07	3.5130	3.33			
72	RX J0457.0+3142	0.05	0.24	55.95	>37.6	>> 9		55.95
73	RX J0457.2+1524	0.06	0.12	1.72	2.39			
75	RX J0458.7+2046	0.06	0.14	7.741	7.53			7.741

Note. bo97: Bouvier et al. (1997); br06: Broeg et al. (2006);
xi06: Xing et al. (2006); gr08: Grankin et al. (2008).

ROTATIONAL MODULATION

Thirty nine stars from Wichmann’s sample show periodic light variations during one or more seasons. To increase our sample of magnetically active stars with known rotation periods, we used data for 22 WTTS from Grankin et al. (2008). Owing to such a combination, the sample of stars with known rotation periods toward the Taurus–Auriga SFR reached 61 objects. Analysis of the distribution (histogram) of rotation periods for 61 stars from the combined list showed that the rotation periods lie within the range from 0.5 to 10 days. In this case, 50 stars ($\sim 82\%$) exhibit periodic variations in the range from 0.5 to 4.5 days and only 11 stars ($\sim 18\%$) have rather long rotation periods in the range from 5 to 10 days. Below, we will call these two groups of stars rapidly and slowly rotating ones. The distribution of periods among the rapidly rotating stars has a noticeable deficit of objects with periods of about 2 days. This deficit is noticeable both among the stars from Wichmann’s list and among the stars from Grankin’s list.

Analysis of our long-term observations revealed significant differences between the photometric behaviors of WTTS from Grankin’s and Wichmann’s lists. Among the 22 spotted WTTS from Grankin’s list, there are six stars with record amplitudes of periodic light variations reaching $0.^m4 - 0.^m8$. in the V band. All these six most active stars show stability of the phase of minimum light (φ_{\min}) over 5–19 years of observations (Grankin et al. 2008).

We performed a similar analysis for our long-term observations of 39 spotted stars from

Wichmann’s list and could not find the objects among them that exhibited stability of φ_{\min} over 6–11 years or that showed significant photometric variability amplitudes as did the known WTTS. The maximum amplitude of periodic light variations observed in the stars from Wichmann’s list was no more than $0.^m28$ (star N7). And only two objects (N63 and N75) show stability of φ_{\min} over 3–4 seasons (see Fig. 2).

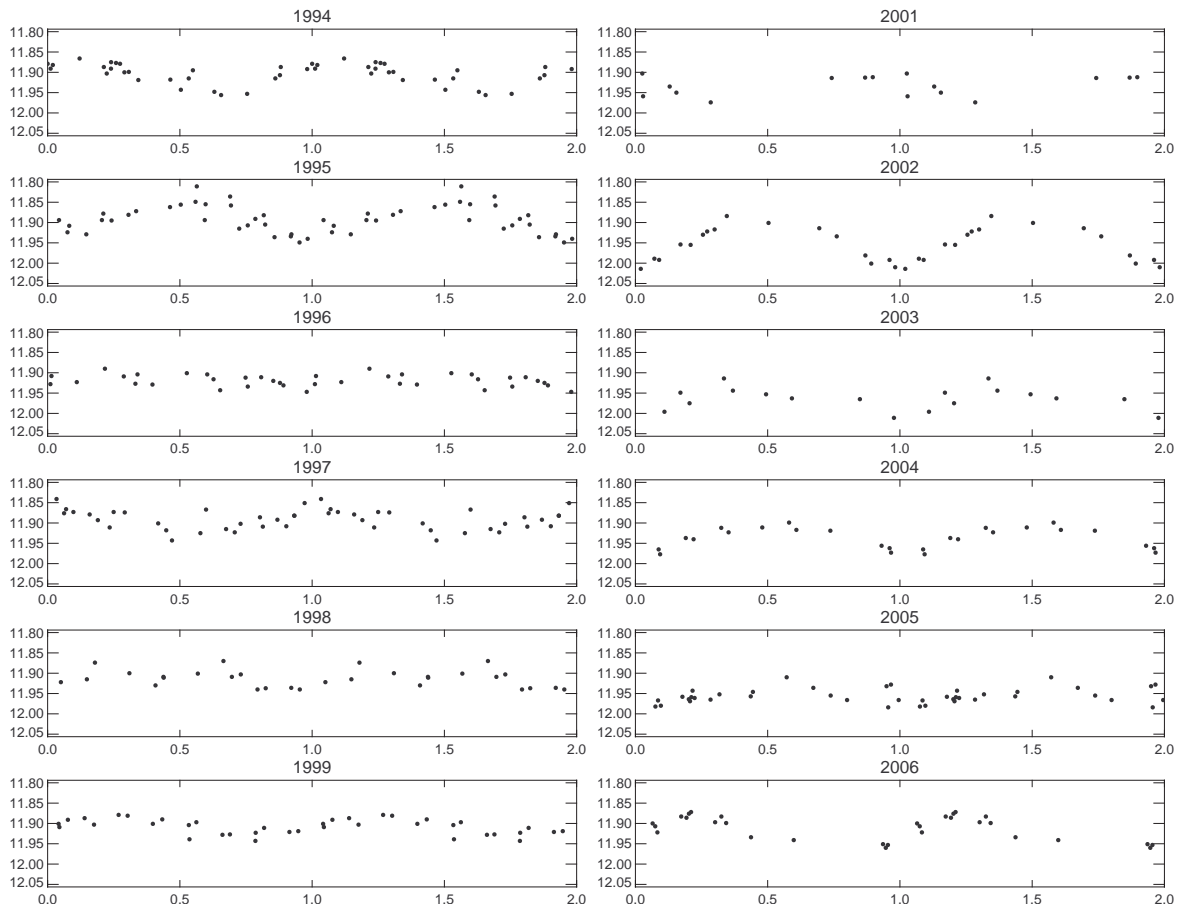


Figure 2: Phase light curves for RX J0458.7+2046 (number 75 in Wichmann’s list) for each individual season. Periodic light variations were observed during at least nine seasons. The phase light curve retains the phase of minimum light for 4 years (from 2002 to 2005).

There is one more significant difference between the photometric behaviors of WTTS from Grankin’s list and Wichmann’s lists. The stars from Wichmann’s list exhibit periodic light variations not so often as do WTTS. As a criterion for the frequency of occurrence of a periodicity, we used a simple parameter $f = (N_p/N_t) \times 100\%$, where N_p is the number of observing seasons with periodic light variations and N_t is the total number of observing seasons. Thus, the most active WTTS mentioned above show periodic variations in almost every observing season, i.e., $f = 90 - 100\%$. Other, less active WTTS exhibit periodic variations with a mean frequency of 68%.

In contrast, the mean frequency of occurrence of periodic variations in the stars from Wichmann’s list does not exceed 50%, i.e., periodic variations are observed in half the observing seasons. Only five stars showed a fairly frequent occurrence of periodic variations: N63, N75, N28, N67, and N32, with $f = 83, 73, 67, 67,$ and 64% , respectively. We hypothesize that such significant differences in the photometric behavior of WTTS from Grankin’s and Wichmann’s

lists stem from the fact that these two subgroups of stars show different activity levels and/or have slightly different ages.

DETERMINATION OF STELLAR PROPERTIES

To place the object under study on the Hertzsprung– Russell (HR) diagram and to estimate its mass and age, its effective temperature and bolometric luminosity should be determined with the maximum possible accuracy.

Effective Temperature

We estimated T_{eff} from the spectral types reported by Wichmann et al. (1996) using the temperature calibration between the spectral type and T_{eff} for main-sequence stars from Tokunaga (2000). Before choosing this calibration, we analyzed several different temperature scales for main-sequence stars from Bessell (1991), Cohen and Kuhn (1979), de Jager and Nieuwenhuijzen (1987), Kenyon and Hartmann (1995), and Tokunaga (2000). The general form of these scales is shown in Fig. 3, where the T_{eff} – spectral type diagram is presented. A detailed description of these scales and estimates of their intrinsic errors can be found in Ammler et al. (2005). Analysis showed that the systematic shifts between different temperature scales could reach 160–210 K and 220–260 K for spectral types G4–G9 and M4–M7, respectively. In this case, the intrinsic errors of the temperature scales are comparable to these systematic shifts (see Table 2 in Ammler et al. (2005)).

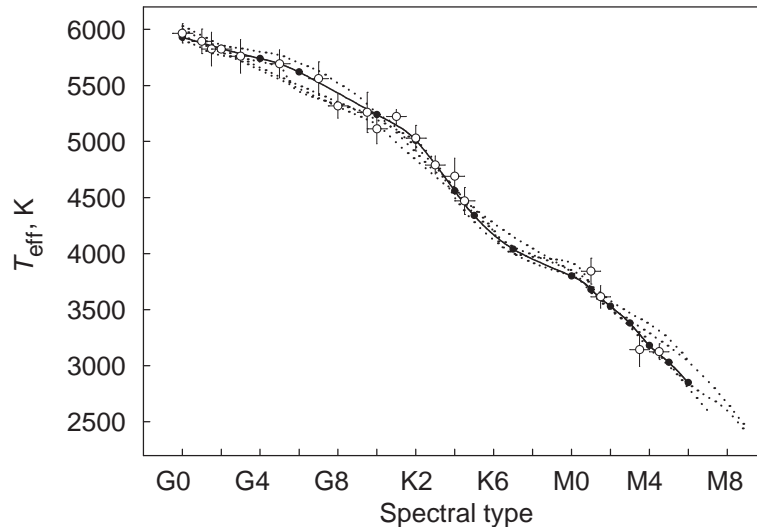


Figure 3: General form of the temperature scales on the spectral type versus effective temperature diagram. The calibration from Tokunaga (2000) is indicated by the black circles connected by the solid line. The remaining calibrations are indicated by the dotted lines. The white circles with error bars represent the averaged experimental data from Torres et al. (2010).

To choose the most acceptable temperature scale from these five scales, we used experimental data on the temperatures and spectral types of 43 G0– M4.5 dwarfs from Torres et al. (2010). All these stars are the components of noninteracting eclipsing binaries for which the mass and radius are known with an accuracy of $\pm 3\%$ or better. Torres et al. (2010) point out that T_{eff} for these stars have typical errors of $\sim 2\%$. We sorted these 43 stars according their spectral types and calculated the mean T_{eff} for each individual subtype. In Fig. 3, these mean T_{eff}

are designated by the white circles. A further analysis showed that the mean T_{eff} calculated from the experimental data from Torres et al. (2010) agree with the temperature calibration from Tokunaga (2000) much better than with the remaining calibrations. Indeed, the scatter of mean T_{eff} relative to the calibration from Tokunaga (2000) is minimal, with an error of ± 85 K. In Fig. 3, the calibration from Tokunaga (2000) is designated by the black circles connected by the solid line.

Wichmann et al. (2000) estimate the accuracy of the spectral classification for bright stars to be about ± 0.8 subtype for G and K stars and about ± 0.5 subtype for M stars. If we use the temperature calibration from Tokunaga (2000) and take the uncertainty in the spectral classification for faint stars to be ± 1 subtype, then the corresponding uncertainty in T_{eff} will be ± 50 K for G1–G6 stars, ± 100 K for G7–K1, ± 195 K for K2–K6, ± 90 K for K7–M0, and ± 160 K for M1–M6.

Bolometric Luminosity

As a rule, the stellar bolometric luminosity (L_{bol}) is very difficult to determine, because T Tauri stars often have optical and near-infrared excesses attributable to the presence of accretion disks. In our case, these problems do not arise, because the objects of our sample show neither infrared excesses nor optical excess emission. This implies that we can determine L_{bol} by assuming the entire flux in the V and R bands to come from the stellar photosphere and calculate the extinction A_V from the color excess as $E_{V-R} = (V - R) - (V - R)_o$, where $(V - R)$ is the color of the observed star and $(V - R)_o$ is the color of a standard star of the corresponding spectral type (Kenyon and Hartmann 1995). Using the standard extinction law (Johnson 1968), we obtained $A_V = 3.7E_{V-R}$ for Johnson’s V and R bands.

Finally, L_{bol} was calculated using the well-known formula $\log(L_*/L_\odot) = -0.4(V_{\text{max}} - A_V + BC + 5 - 5 \log r - 4.72)$, where BC is the bolometric correction from Hartigan et al. (1994) and r is the mean distance to the Taurus–Auriga SFR (140 pc).

Sources of Errors in the Luminosity Estimate

There are several sources of significant errors in the L_{bol} estimates: inaccurate photometry, physical photometric variability, inaccurate spectral classification and T_{eff} estimation, errors in the adopted colors for main-sequence dwarfs, the presence of an unresolved component in the binary system, the lack of reliable information about the distance to the object under study, and others. A detailed discussion of the possible errors and the degree of their influence on the determination of physical parameters for stars can be found in Hartigan et al. (1994).

To estimate the magnitude V_{max} and the $V - R$ color, we used highly accurate homogeneous long-term photometry data obtained at the Maidanak Astronomical Observatory, which is known for its excellent astroclimate (see, e.g., Ehgamberdiev et al. 2000). Therefore, V_{max} and $V - R$ were determined with a high accuracy, at least a few thousandths of a magnitude. Owing to such a photometric accuracy, we detected periodic light variations with amplitudes of the order of $0.^m03 - 0.^m05$ in the V band, for example, for RX J0441.8+2658 (see Fig. 1). Thus, the photometric error makes a minor contribution to the error in L_{bol} .

The photometric variability of the stars from our sample is attributable primarily to the existence of extended cool spots. As has been shown above, the stars of our sample exhibit a small variability amplitude between $0.^m05$ and $0.^m15$. To minimize the influence of photometric variability, we used the maximum brightness (V_{max}) and the corresponding color ($V - R$). Indeed, at the time of maximum light the visible stellar surface is least covered with spots.

Therefore, its brightness and color most closely correspond to a pure photosphere. Thus, we minimized the influence of photometric variability on the L_{bol} estimate.

Considerably more serious errors can be caused by the possible existence of an unresolved secondary component and the uncertainty in the adopted distance. Thus, the uncertainty due to unresolved binary systems can imply that we overestimate L_{bol} by a factor of 2 in the worst case. A no less serious problem is related to the uncertainty in the distance. Since the evolutionary status of the stars from our sample is still unclear and is being actively discussed, their membership in the Taurus–Auriga SFR has not been proven. Therefore, we cannot assert with confidence that all stars of our sample are at a mean distance of 140 pc. Thus, according to Hipparcos data, the distance to RX J0406.7+2018 (star N6) is 156 pc, while the distance to RXJ0441.8+2658 (star N50) is only 115 pc. This implies that, depending on the adopted distance (140 or 156 pc in the former case and 140 or 115 pc in the latter case), the relative error in L_{bol} can reach tens of percent. The uncertainty in the distances to these two stars can lead to an error in $\log L_{\text{bol}}$ of the order of $\pm 0.1 - 0.17$ dex.

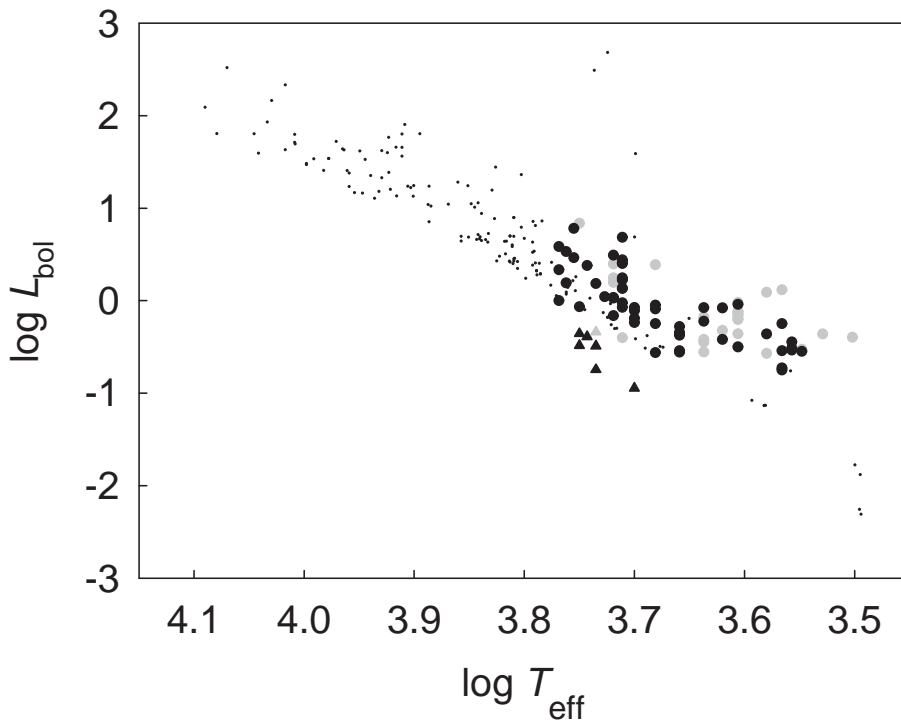


Figure 4: Effective temperature–luminosity diagram. About 190 objects from Torres et al. (2010) are marked by the black dots. The filled black and gray circles represent the stars from Wichmann’s and Grankin’s lists, respectively. The objects with underestimated luminosities are designated by the black and gray triangles, respectively.

To reveal the stars with definitely underestimated L_{bol} , we used the $T_{\text{eff}} - L_{\text{bol}}$ diagram presented in Fig. 4. About 190 objects from Torres et al. (2010) are marked by the black dots. Since the luminosities of these 190 stars are known with a high accuracy (at least ± 0.05 dex), we compared their positions on the diagram with those of the stars from Wichmann’s list (black filled circles) and Grankin’s list (gray filled circles). Most of the stars from our two lists occupy the same region on the diagram as do the stars from the list by Torres et al. (2010). However, there are seven stars located slightly below the main relation. We designated them by the black and gray triangles (N19, N38, N49, N51, N61, N65, and TAP 49). Since these stars are most likely located appreciably farther than 140 pc, L_{bol} were underestimated for them.

Radius

The stellar radii were determined by several methods. First, we estimated the radii (R_{bol}) using T_{eff} and L_{bol} .

Second, we used the ratio from Kervella and Fouqué (2008). These authors gathered the existing interferometric measurements and broadband photometry of the nearest dwarfs and subgiants and obtained polynomial relations between the angular diameters of these stars and their visible colors. In particular, they showed that the angular diameter could be estimated with an accuracy of at least 5%. We estimated the stellar radii (R_{KF}) using the Kervella–Fouqué calibration by assuming the mean distance to the Taurus–Auriga SFR to be ≈ 140 pc.

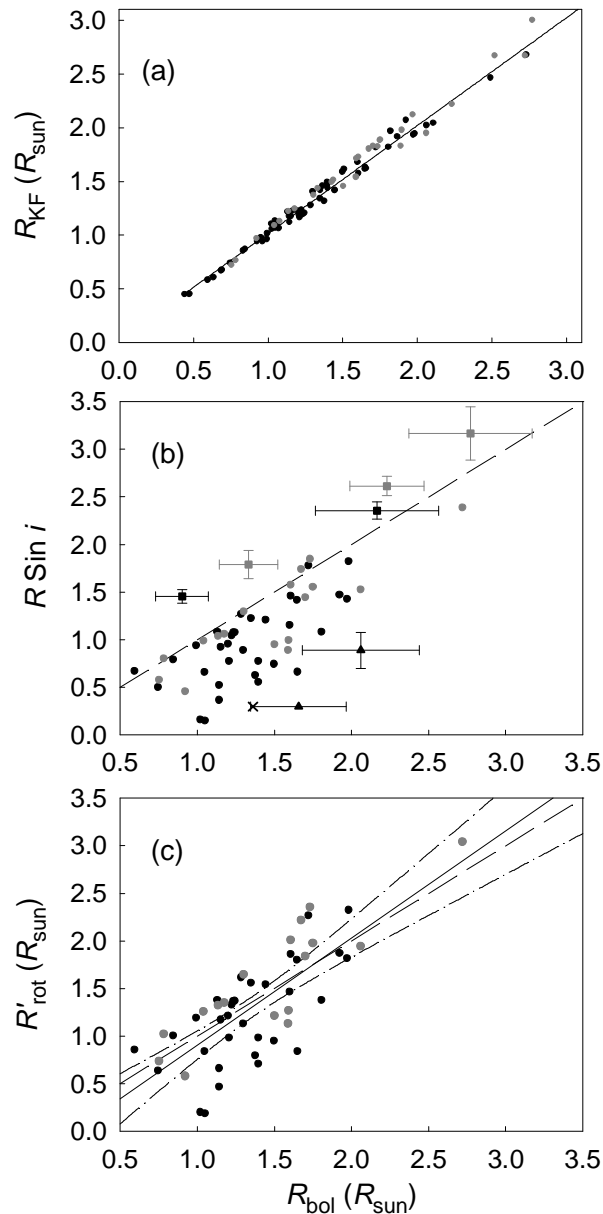


Figure 5: Comparison of the stellar radii R_{bol} obtained using L_{bol} and T_{eff} with the radii R_{KF} derived from the Kervella–Fouqué relation (a), with the $R \sin i$ estimate (b), and with the R'_{rot} estimate (c). The black and gray circles indicate the stars from Wichmann’s and Grankin’s lists, respectively. The objects with underestimated and overestimated R_{bol} are designated by the squares and triangles, respectively. The cross indicates the position of object N50 for a distance of 115 pc (for details, see the text).

The stellar radii determined by these two methods are compared in Fig. 5a. The estimated radii are in good agreement with the mean ratio $\langle R_{\text{KF}}/R_{\text{bol}} \rangle = 1.004 \pm 0.012$.

There is one more possibility for an independent estimation of the stellar radii without using the distance, L_{bol} , and T_{eff} . For the stars with measured $v \sin i$ and known rotation periods P_{rot} , we can estimate the radii as $R \sin i = (P_{\text{rot}} \times v \sin i)/2\pi$. In Fig. 5b, R_{bol} are compared with $R \sin i$. Since $\sin i \leq 1$, the following relation must hold: $R \sin i \leq R_{\text{bol}}$. The dashed line corresponds to the condition $R \sin i = R_{\text{bol}}$. It can be seen from the figure that this condition holds for most of the stars, with the exception of two stars from Wichmann’s list (N52 and N55) and three stars from Grankin’s list (LkCa 3, V410 Tau, and V836 Tau). They lie well above the dashed line and are designated by the black and gray squares, respectively. Since $R \sin i$ are known with greater reliability than R_{bol} , it should be recognized that R_{bol} were grossly underestimated for these five stars. There are two possible reasons for this underestimation: either the distance to these objects is greater than 140 pc or V_{max} used to calculate R_{bol} were underestimated. If these five stars are assumed to be seen face-on, i.e., $\sin i = 1$, then the minimum admissible distance to these objects cannot be less than 225, 161, 160, 165, and 168 pc, respectively.

However, this assumption is unacceptable for V410 Tau, because the distance to this object is known with a good accuracy and does not exceed 137 ± 17 pc (Bertout and Genova 2006). The discrepancy between R_{bol} and $R \sin i$ suggests that even when we observe the star in its brightest state, it still has significant spots on the visible surface. In other words, the true “unspotted” magnitude of this star can be brighter than $V_{\text{max}} = 10.^m57$. In particular, Grankin (1999) calculated the absolute unspotted magnitude of V410 Tau, which is brighter than the recorded V_{max} by $0.^m33$. In this case, $R_{\text{bol}} \simeq 2.6R_{\odot}$, which corresponds to $R \sin i$ at a mean distance of about 140 pc. A similar explanation of the discrepancy between R_{bol} and $R \sin i$ can also be valid for V836 Tau, whose photosphere is heavily spotted (Grankin 1998).

There are two other stars (N28 and N50) for which R_{bol} is considerably larger than $R \sin i$. They are located in the lower part of the figure and are designated by the black triangles. It may well be that L_{bol} and R_{bol} were overestimated for these two objects because of the distance overestimation or due to the existence of unresolved components. According to Hipparcos data, the distance to star N50 is 115 ± 18 pc. If we estimate R_{bol} for this distance, then the star will be displaced on the plot leftward, closer to the main group of stars (cross). It may well be that the second star (N28) also lies at a closer distance. On the other hand, Kohler and Leinert (1998) reported that star N28 consists of four components, while star N50 is a triple system. Therefore, R_{bol} could be overestimated, because the contribution from several fairly bright components was ignored.

For a randomly oriented sample of stars, the mean $\langle \sin i \rangle = \pi/4$ and the stellar radius can be estimated as $R'_{\text{rot}} = R \sin i / \langle \sin i \rangle = (2P_{\text{rot}} \times v \sin i) / \pi^2$. R_{bol} and R'_{rot} are compared in Fig. 5c. The solid line indicates a linear fit to the data with the mean ratio $\langle R'_{\text{rot}}/R_{\text{bol}} \rangle = 1.125 \pm 0.096$. The dash-dotted lines indicate the 95% confidence region for this linear relation. The dashed line corresponds to the condition $R \sin i = R_{\text{bol}}$. We excluded the seven stars discussed above from our regression analysis. It can be seen from the figure that the regression relation is steeper than the dashed line that corresponds to the condition $R'_{\text{rot}} = R_{\text{bol}}$. This difference can result from a systematic underestimation of R'_{rot} for stars with small inclinations, when $\sin i \ll \pi/4$.

To reveal the stars with underestimated R'_{rot} , we used the $T_{\text{eff}} - R'_{\text{rot}}$ diagram presented in Fig. 6. About 190 objects from Torres et al. (2010) are marked by the black dots. Since the radii of these objects are known with a high accuracy (at least $\pm 3\%$), we compared their positions on the diagram with those of the stars from our sample. Most of the stars from our sample occupy the same region on the diagram as do the stars from the list by Torres et al.

(2010). They are designated by the black and gray circles. However, there are eight stars from Wichmann’s list and two stars from Grankin’s list that are located well below the main relation. They are marked by the black and gray triangles. Since these stars most likely have small inclinations ($\sin i \ll \pi/4$), R'_{rot} were clearly underestimated for them.

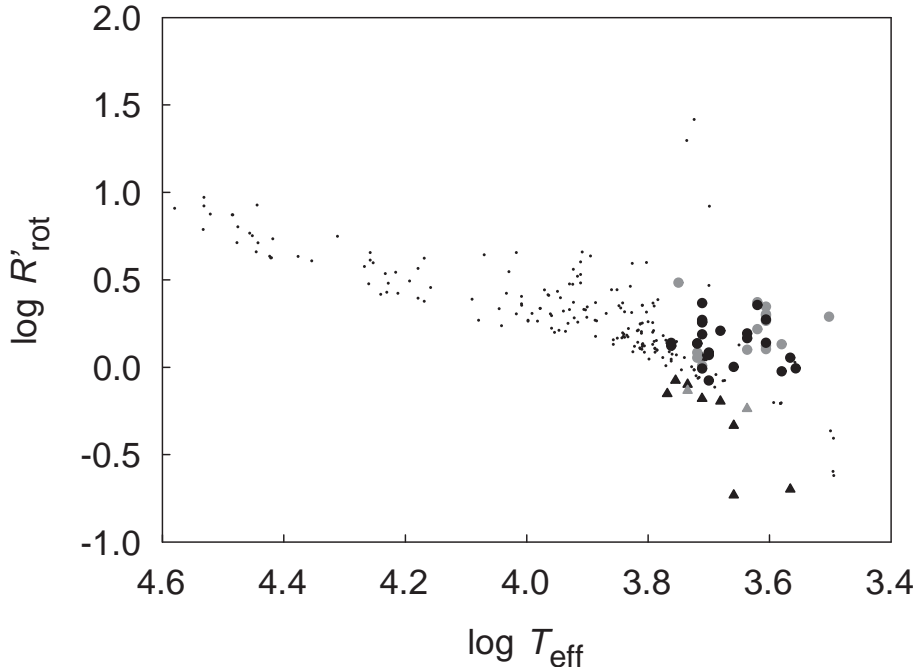


Figure 6: $T_{\text{eff}} - R'_{\text{rot}}$ diagram. About 190 objects from Torres et al. (2010) are marked by the black dots. The stars with reliable R'_{rot} are designated by the black and gray circles, while those with underestimated values are designated by the black and gray triangles.

Thus, we were able to identify 24 objects with reliable R'_{rot} estimates and known rotation periods among the stars from Wichmann’s list. Note that these estimates do not depend on the adopted distance. Since the distance plays a key role in determining L_{bol} , we attempted to estimate the mean distance to these 24 stars using reliable R'_{rot} estimates. Initially, we calculated the luminosities of these stars using R'_{rot} , T_{eff} , and the Stefan–Boltzmann law. Subsequently, we estimated the distance to each star using V_{max} and A_V . Finally, we calculated the mean distance to these 24 stars using the individual distance estimates. The mean distance to these stars turned out to be 143 ± 26 pc and to be in excellent agreement with the adopted distance to the Taurus–Auriga SFR. Consequently, we can assert that using the distance $r = 140$ pc is quite justified when calculating the basic physical parameters of the stars from Wichmann’s list.

Hertzsprung–Russell Diagram

To estimate the masses and ages of the magnetically active stars, we used the grid of evolutionary tracks for pre-main-sequence stars computed by Siess et al. (2000). The Hertzsprung–Russell (HR) diagrams are presented in Fig. 7. For greater clarity, we show two separate HR diagrams: one for the stars with reliable rotation periods (P_{rot}) and $v \sin i$ (Fig. 7a) and the other for the stars without reliable P_{rot} or $v \sin i$ (Fig. 7b). For comparison, the diagram also shows the positions of known WTTS from Grankin’s list (gray color). The errors in the mass and age depend on the uncertainties in T_{eff} and L_{bol} adopted in this study and on the object’s position on

the HR diagram. The error in the mass is $\pm 0.1 M_{\odot}$ and $\pm 0.2 M_{\odot}$ for the objects on convective and radiative tracks, respectively. The error in the age is of the order of $\pm 1 - 4$ Myr.

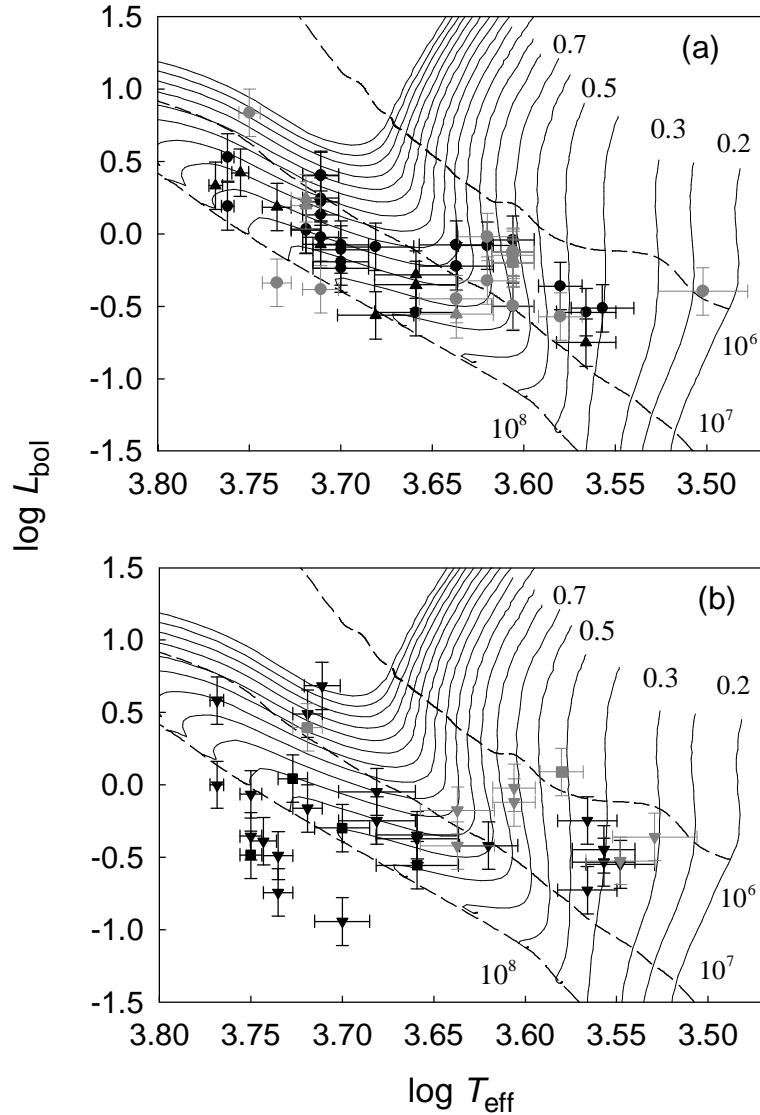


Figure 7: HR diagram for the stars with reliable P_{rot} and $v \sin i$ (a) and for the remaining stars (b). The black and gray circles represent all stars with reliable P_{rot} and good R'_{rot} estimates; the black and gray triangles represent the stars with reliable P_{rot} and underestimated R'_{rot} ($v \sin i < 0.67$). The black and gray squares represent the stars with reliable P_{rot} but without $v \sin i$; the black and gray overturned triangles represent the stars without reliable P_{rot} . The errors indicate the $\pm 1\sigma$ uncertainty for L_{bol} and T_{eff} . The solid black lines indicate the evolutionary tracks computed with $Y = 0.277$ and $Z = 0.02$ for stars with masses in the range from 0.2 to $2 M_{\odot}$ with a mass increment of $0.1 M_{\odot}$. The dashed lines indicate the isochrones for ages of 10^6 , 10^7 , and 10^8 yr.

The stars from Wichmann’s list have masses in the range from $0.4 M_{\odot}$ to $2.2 M_{\odot}$ and ages from 1.5 to 100 Myr. About 33% of the stars have ages younger than 10 Myr. Seven stars lie well below the main sequence on the HR diagram. Their optical spectra exhibit the $H\alpha$ line in absorption and they are G6–G8 dwarfs (only one star is of spectral type K2). For these seven stars to be above the main sequence, their $\log L_{\text{bol}}$ must be corrected by more than 0.30–0.55 dex and, consequently, they must be located at distances of ~ 200 –280 pc.

All of the basic parameters for the stars from Wichmann’s and Grankin’s lists and the

intermediate data used for their calculations are presented in Tables 3 and 4, respectively. The stars without reliable data on their luminosities, radii, masses, and ages are presented in Table 5. The rotation periods were taken from Grankin et al. (2007a, 2008) and Table 2. The values of $v \sin i$ were taken from Sartoretti et al. (1998), Wichmann et al. (2000), Clarke and Bouvier (2000), Massarotti et al. (2005), and Nguyen et al. (2009).

CONCLUSIONS

We analyzed homogeneous long-term photometric observations of 28 well-known WTTS in the Taurus–Auriga SFR from Grankin’s list (see Grankin et al. 2008) and 60 WTTS candidates from Wichmann’s list (see Wichmann et al. 1996) and obtained the following results.

Most of the stars from Wichmann’s list (97%) exhibit small photometric variability amplitudes in the V band between $0.^m05$ and $0.^m15$. The mean brightness level changes from season to season insignificantly ($\sigma_{V_m} \leq 0.^m06$). Similarly, the changes in the photometric amplitude ($\sigma_{\Delta V}$) from season to season are small for most stars ($<0.^m06$).

We showed that 39 stars from Wichmann’s list exhibit periodic light variations attributable to the phenomenon of spotted rotational modulation. We analyzed the rotation periods for 39 stars from Wichmann’s list and 22 well-known WTTS from Grankin’s list. Owing to this combination, the sample of magnetically active stars with known rotation periods toward the Taurus–Auriga SFR reached 61 objects. The rotation periods of the magnetically active stars lie within the range from 0.5 to 10 days; 50 stars ($\sim 82\%$) exhibit periodic variations within the range from 0.5 to 4.5 days and only 11 stars ($\sim 18\%$) have fairly long rotation periods in the range from 5 to 10 days.

We found significant differences between the long-term photometric behaviors of 22 WTTS from Grankin’s list and 39 stars from Wichmann’s list. There are no very active stars that would exhibit large amplitudes of periodic light variations and stability of the phase of minimum light among the objects from Wichmann’s list. In addition, the stars from Wichmann’s list exhibit periodic light variations not so often as do the known WTTS. Thus, the most active WTTS from Grankin’s list show periodic variations in almost every observing season, i.e., with a frequency $f = 90 - 100\%$. Other, less active WTTS exhibit periodic variations with a mean frequency of $\sim 68\%$. In contrast, the mean detection frequency of periodic variations in the stars from Wichmann’s list does not exceed 50%, i.e., periodic light variations are observed in no more than half the observing seasons. We hypothesize that such differences in the photometric behavior of the known WTTS and stars from Wichmann’s list are explained by the fact that these two subgroups of stars show different activity levels and/or have slightly different ages.

For all stars, we estimated T_{eff} using the temperature calibration from Tokunaga (2000). We showed that the errors in the effective temperature could reach ± 50 K for G1–G6 stars, ± 100 K for G7–K1, ± 195 K for K2–K6, ± 90 K for K7–M0, and ± 160 K for M1–M6.

We calculated the stellar luminosity L_{bol} by assuming all stars to be at the mean distance of the Taurus–Auriga SFR. We discussed the various sources of errors in the L_{bol} estimates and attempted to minimize some of these errors. We showed that the errors in $\log L_{\text{bol}}$ could reach $\pm 0.1 - 0.17$ dex. Using the $T_{\text{eff}} - L_{\text{bol}}$ diagram constructed for 190 stars from Torres et al. (2010) with well-known T_{eff} and L_{bol} , we were able to reveal seven stars with definitely underestimated L_{bol} .

The stellar radii were estimated by three different methods: using L_{bol} and T_{eff} (R_{bol}), using the Kervella–Fouqué ratio (R_{KF}), and via P_{rot} and $v \sin i$ (R'_{rot}). The estimates of R_{bol} and R_{KF} were shown to be in excellent agreement. We revealed five stars with overestimated R_{bol} ($R_{\text{bol}} \gg R \sin i$) and two stars with underestimated R_{bol} ($R_{\text{bol}} \ll R \sin i$). The possible

Table 3: Basic parameters of the WTTS candidates and the intermediate data used for their calculations. The mass and age estimates were obtained in comparison with the theoretical models and tracks computed by Siess et al. (2000)

W96	V_{\max}	$V - R$	Sp. type	E_{V-R}	A_V	B.C.	$v \sin i$ (km c^{-1})	P_{rot} (days)	T_{eff} (K)	L_{bol} (L_{\odot})	R (R_{\odot})	M (M_{\odot})	t , 10^6 (yr)
1	10.144	0.804	K1	0.12	0.46	-0.25	79	1.1683	5145	2.55	1.98	1.60	7.24
2	11.616	0.943	K3	0.14	0.53	-0.41	112	0.573	4801	0.81	1.28	1.15	14.60
3	11.229	0.740	K2	0.00	0.00	-0.30	17	1.961	5010	0.64	1.05	0.98	28.40
4	10.327	0.745	K1	0.06	0.24	-0.25	25	2.86	5145	1.76	1.65	1.40	10.50
5	9.310	0.558	G3	0.03	0.10	-0.08	67	0.816	5786	3.39	1.81	1.38	14.40
6	9.667	0.517	G1	0.00	0.00	-0.06	26	1.079	5876	2.15	1.40	1.22	21.20
7	11.834	1.256	K7	0.11	0.39	-0.89	44	1.6906	4040	0.91	1.92	0.73	1.96
8	11.482	0.800	K3	0.00	0.00	-0.41	24		4801	0.56	1.07	1.00	23.50
10	10.494	0.713	K1	0.03	0.12	-0.25	23	2.662	5145	1.35	1.44	1.28	14.60
11	13.266	1.403	M1	0.00	0.01	-1.45	73	0.616	3680	0.29	1.30	0.45	3.27
12	13.420	1.478	M1.5	0.03	0.10	-1.58	7	5.58	3605	0.31	1.40	0.40	2.45
13	12.526	1.142	K6	0.07	0.27	-0.76	12		4166	0.38	1.16	0.91	11.00
14	11.960	1.003	G9	0.39	1.46	-0.16	-	0.865	5337	1.10	1.21	1.09	23.40
15	10.947	0.638	G1	0.12	0.44	-0.06	9		5876	1.00	0.95	1.20	100
18	10.557	0.640	K0	0.00	0.00	-0.19	30	1.812	5240	1.08	1.24	1.12	22.40
23	12.478	0.941	K4	0.04	0.15	-0.52	9	4.429	4560	0.29	0.85	0.83	37.95
27	11.192	0.786	K2	0.05	0.17	-0.30	29	1.605	5010	0.78	1.15	1.07	22.70
29	11.293	1.148	K0	0.51	1.88	-0.19	55		5240	3.10	2.11	1.67	7.01
30	9.343	0.540	G5	0.00	0.00	-0.09	48	0.6962	5687	3.01	1.76	1.35	14.60
31	10.277	0.623	G8	0.04	0.16	-0.13	43	0.736	5438	1.53	1.38	1.20	18.70
32	10.704	0.675	K0	0.04	0.13	-0.19	20	2.7136	5240	1.06	1.23	1.11	22.40
36	10.761	0.680	K1	0.00	0.00	-0.25	25	1.561	5145	0.95	1.21	1.10	21.40
37	13.712	1.548	M2	0.05	0.18	-1.71	11		3530	0.28	1.40	0.37	2.38
39	12.051	0.911	G6	0.36	1.34	-0.10	-		5620	0.86	0.96	1.10	100
40	13.374	1.511	M1.5	0.06	0.23	-1.58	6		3605	0.36	1.51	0.40	2.02
41	13.135	1.232	K4	0.33	1.23	-0.52	10		4560	0.42	1.03	0.95	23.00
44	12.141	0.955	K2	0.22	0.80	-0.30	16	2.96	5010	0.58	0.99	0.95	32.30
45	13.788	1.418	M1	0.02	0.07	-1.45	8		3680	0.19	1.05	0.44	5.66
46	13.234	1.061	K3	0.26	0.97	-0.41	10	2.535	4801	0.27	0.75	0.84	100
47	10.792	0.855	K1	0.18	0.65	-0.25	24	3.0789	5145	1.67	1.60	1.38	11.60
48	11.397	1.027	K5	0.04	0.14	-0.62	24	2.425	4340	0.84	1.60	1.10	4.91
53	12.526	1.401	M1	0.00	0.00	-1.45	7		3680	0.56	1.82	0.45	1.44
54	9.490	0.815	K1	0.14	0.50	-0.25	80		5145	4.83	2.73	2.05	3.83
56	12.802	1.355	M0	0.08	0.28	-1.17	10	3.762	3800	0.44	1.50	0.53	2.49
57	12.362	0.995	K0	0.36	1.31	-0.19	27		5240	0.69	0.99	0.96	35.20
58	11.166	0.757	K1	0.08	0.29	-0.25	55	0.4778	5145	0.85	1.14	1.05	25.10
59	13.893	1.592	M1.5	0.14	0.53	-1.58	17		3605	0.29	1.36	0.40	2.60
60	13.281	1.148	K4	0.25	0.92	-0.52	-	0.921	4560	0.28	0.83	0.82	43.90
62	12.000	0.940	K4	0.04	0.15	-0.52	9	0.8204	4560	0.44	1.05	0.98	22.00
63	11.626	1.128	K6	0.06	0.21	-0.76	26	3.46	4166	0.83	1.72	0.89	3.13
64	12.054	0.958	K4	0.06	0.21	-0.52	6		4560	0.45	1.06	0.98	21.20
66	9.192	0.558	G1	0.04	0.14	-0.06	81		5876	3.83	1.87	1.40	14.20
67	11.153	0.846	K3	0.05	0.17	-0.41	19		4801	0.89	1.35	1.20	13.00
68	12.595	1.150	K7	0.00	0.00	-0.89	9.7	5.64	4040	0.31	1.13	0.80	10.20
70	14.234	1.524	M1	0.12	0.46	-1.45	9	0.884	3680	0.18	1.02	0.44	6.00
71	10.293	0.595	G3	0.06	0.24	-0.08	15	3.513	5786	1.55	1.22	1.16	25.40
73	10.200	0.816	K1	0.14	0.50	-0.25	42	1.72	5145	2.52	1.97	1.60	7.24
74	10.995	0.756	K2	0.02	0.06	-0.30	33	1.46	5010	0.84	1.20	1.10	20.10
75	11.841	1.047	K5	0.06	0.21	-0.62	8	7.741	4340	0.60	1.35	1.06	8.23
76	11.685	0.903	K4	0.00	0.01	-0.52	15	1.2308	4560	0.52	1.14	1.05	16.40

Table 4: Basic parameters of the known WTTS and the intermediate data used for their calculations. The mass and age estimates were obtained in comparison with the theoretical models and tracks computed by Siess et al. (2000)

Name	V_{\max}	$V - R$	Sp. type	E_{V-R}	A_V	B.C.	$v \sin i$ (km c^{-1})	P_{rot} (days)	T_{eff} (K)	L_{bol} (L_{\odot})	R (R_{\odot})	M (M_{\odot})	$t, 10^6$ (yr)
Anon 1	13.374	1.814	M0	0.53	1.98	-1.17		6.493	3800	1.23	2.52	0.52	0.81
HD283572	8.914	0.673	G6	0.12	0.46	-0.10	79	1.529	5620	6.87	2.72	1.84	6.26
LkCa 1	13.681	1.700	M4	0.00	0.00	-2.24	30.9	2.497	3180	0.40	2.06	0.24	0.37
LkCa 4	12.285	1.297	K7	0.15	0.54	-0.89	26.1	3.374	4040	0.74	1.73	0.74	2.60
LkCa 5	13.476	1.500	M2	0.00	0.00	-1.71	37		3530	0.30	1.44	0.37	2.26
LkCa 7	12.144	1.268	K7	0.12	0.44	-0.89	12.9	5.6638	4040	0.71	1.70	0.74	2.70
LkCa 14	11.641	1.025	K5	0.03	0.13	-0.62	21.9		4340	0.67	1.43	1.09	7.00
LkCa 16	12.335	1.405	K7	0.26	0.94	-0.89	6.9		4040	0.96	1.97	0.72	1.81
LkCa 19	10.807	0.851	K0	0.21	0.78	-0.19	20.1	2.236	5240	1.76	1.59	1.34	12.80
LkCa 21	13.451	1.648	M3	0.05	0.18	-1.92	60		3380	0.44	1.89	0.31	1.40
TAP 4	12.164	0.804	K1	0.12	0.46	-0.25	83.9	0.482	5145	0.40	0.78	0.89	73.00
TAP 9	12.122	0.990	K5	0.00	0.00	-0.62	36		4340	0.38	1.08	0.95	16.60
TAP 26	12.194	0.990	K5	0.00	0.00	-0.62	70	0.7135	4340	0.36	1.04	0.93	18.60
TAP 35	10.174	0.647	K0	0.01	0.03	-0.19	17.6	2.734	5240	1.57	1.50	1.28	14.50
TAP 40	12.535	1.011	K5	0.02	0.08	-0.62	14.8	1.5548	4340	0.28	0.92	0.86	26.20
TAP 41	12.028	1.073	K6	0.00	0.01	-0.76	27	2.425	4166	0.48	1.30	0.92	8.14
TAP 45	13.135	1.299	K7	0.15	0.55	-0.89	5.3	9.909	4040	0.32	1.14	0.79	10.00
TAP 50	10.091	0.759	K0	0.12	0.44	-0.19		3.039	5240	2.49	1.89	1.54	8.70
TAP 57	11.530	1.106	K6	0.04	0.13	-0.76	10	9.345	4166	0.95	1.85	0.88	2.43
V819 Tau	12.796	1.405	K7	0.26	0.94	-0.89	9.1	5.53113	4040	0.62	1.59	0.76	3.30
V826 Tau	12.069	1.265	K7	0.12	0.43	-0.89	4.2		4040	0.76	1.75	0.74	2.50
V827 Tau	12.242	1.311	K7	0.16	0.60	-0.89	20.9	3.75837	4040	0.76	1.75	0.74	2.50
V830 Tau	11.933	1.177	K7	0.03	0.10	-0.89	29.1	2.74101	4040	0.64	1.61	0.75	3.13
VY Tau	13.541	1.413	M0	0.13	0.49	-1.17	10	5.36995	3800	0.27	1.18	0.54	5.10

Table 5: List of stars without reliable data on their luminosities, radii, masses, and ages

W96/name	V_{\max}	V-R	Sp. type	E_{V-R}	A_V	B.C.	$v \sin i$ (km c^{-1})	P_{rot} (days)	T_{eff} (K)	Notes
9	12.859	1.107	K2	0.37	1.36	-0.30	75	3.0093	5010	eclipsing binary
19	12.347	0.795	G6	0.25	0.91	-0.10	31		5620	below MS, $r > 210$ pc
28	11.346	1.151	K1	0.47	1.74	-0.25	14	3.21	5145	$R_{\text{bol}} > R \sin i$
38	13.079	0.906	G6	0.36	1.32	-0.10	58	0.5854	5620	below MS, $r > 240$ pc
49	13.060	0.919	G8	0.34	1.26	-0.13	34		5438	below MS, $r > 210$ pc
50	9.613	0.567	G7	0.00	0.00	-0.12	25	0.6	5535	$R_{\text{bol}} > R \sin i$
51	12.831	0.917	G7	0.35	1.29	-0.12	29		5535	below MS, $r > 200$ pc
52	12.594	1.003	K1	0.32	1.20	-0.25	65	1.132	5145	$R_{\text{bol}} < R \sin i$, $r > 225$ pc
55	9.334	0.659	G5	0.12	0.44	-0.09	114	1.104	5687	$R_{\text{bol}} < R \sin i$, $r > 161$ pc
61	14.108	1.009	K2	0.27	1.00	-0.30	47		5010	below MS, $r > 265$ pc
65	13.714	0.923	G8	0.34	1.27	-0.13	-		5438	below MS, $r > 280$ pc
72	10.566	1.310	K2	0.57	2.11	-0.30	27	55.95	5010	$P > P_{\text{rot}}$
LkCa 3	11.978	1.500	M1	0.10	0.37	-1.45	22	7.35	3680	$R_{\text{bol}} < R \sin i$
V410 Tau	10.567	0.983	K3	0.18	0.68	-0.41	71	1.87197	4801	$R_{\text{bol}} < R \sin i$
V836 Tau	13.060	1.372	K7	0.22	0.82	-0.89	12	6.75791	4040	$R_{\text{bol}} < R \sin i$
TAP 49	12.575	0.890	G8	0.31	1.15	-0.13	8.8	3.32	5438	below MS, $r > 180$ pc

causes of the discrepancies between R_{bol} and $R \sin i$ for these seven stars were discussed. The estimates of R_{bol} and R'_{rot} for the stars with known rotation periods P_{rot} and $v \sin i$ were shown to be in excellent agreement with the mean ratio $\langle R'_{\text{rot}}/R_{\text{bol}} \rangle = 1.125 \pm 0.096$. We revealed ten stars with small inclinations ($\sin i \ll \pi/4$) for which R'_{rot} were definitely underestimated. For the remaining 24 stars from Wichmann's list with reliable estimates of R'_{rot} , we calculated the individual distances. The mean distance to these stars was shown to be 143 ± 26 pc, which is in excellent agreement with the adopted distance to the Taurus–Auriga SFR.

The stellar masses and ages were determined for all stars with reliable luminosities. The stars from Wichmann's list were found to have masses in the range from $0.4 M_{\odot}$ to $2.2 M_{\odot}$ and ages from 1.5 to 100 Myr. About 33% of the stars from Wichmann's list have ages younger than 10 Myr and can be members of the Taurus–Auriga SFR.

Owing to this work, there is a sample of 74 magnetically active stars toward the Taurus–Auriga SFR. For all these stars, we determined such basic physical parameters as the luminosities, radii, masses, and ages. For 52 objects we know the rotation periods. Improving the evolutionary status of these objects and investigating the possible relationship between the magnetic activity and rotation of these stars are of indubitable interest. The results of these studies will be presented in two next papers.

ACKNOWLEDGMENTS

The observational part of this work was performed with several telescopes at the Maidanak Astronomical Observatory of the Ulugh Beg Astronomical Institute of the Uzbek Academy of Sciences during 2003–2006 and was supported by the Center for Science and Technologies of Uzbekistan (grant no. F-2-2-3). I wish to thank D. Alekseev, S. Melnikov, B. Kahharov, O. Ezhkova, and S. Artemenko for their participation in the photometric observations.

REFERENCES

01. M. Ammler, V. Joergens, and R. Neuhäuser, *Astron. Astrophys.* **440**, 1127 (2005).
02. C. Bertout and F. Genova, *Astron. Astrophys.* **460**, 499 (2006).
03. M. Bessell, *Astron. J.* **101**, 662 (1991).
04. J. Bouvier, R. Wichmann, K. Grankin, et al., *Astron. Astrophys.* **318**, 495 (1997).
05. C. Broeg, V. Joergens, M. Fernández, et al., *Astron. Astrophys.* **450**, 1135 (2006).
06. C. J. Clarke and J. Bouvier, *Mon. Not. R. Astron. Soc.* **319**, 457 (2000).
07. M. Cohen and L. Kuhi, *Astrophys. J. Suppl. Ser.* **41**, 743 (1979).
08. S. A. Ehgamberdiev, A. K. Bajjumanov, S. P. Ilyasov, et al., *Astron. Astrophys. Suppl. Ser.* **145**, 293 (2000).
09. K. N. Grankin, M. A. Ibragimov, V. B. Kondrat'ev, et al., *Astron. Rep.* **39**, 799 (1995).
10. K. N. Grankin, *Astron. Lett.* **24**, 497 (1998).
11. K. N. Grankin, *Astron. Lett.* **25**, 526 (1999).
12. K. N. Grankin, S. A. Artemenko, and S. Y. Melnikov, *Inform. Bull. Var. Stars*, No. 5752 (2007a).
13. K. N. Grankin, S. Yu. Melnikov, J. Bouvier, et al., *Astron. Astrophys.* **461**, 183 (2007b).
14. K. N. Grankin, J. Bouvier, W. Herbst, et al., *Astron. Astrophys.* **479**, 827 (2008).
15. P. Hartigan, K. M. Strom, and S. E. Strom, *Astrophysics* **427**, 961 (1994).
16. C. de Jager and H. Nieuwenhuijzen, *Astron. Astrophys.* **177**, 217 (1987).
17. H. L. Johnson, in *Nebulae and Interstellar Matter*, Ed. by B. M. Middlehurst and L. H. Aller (Univ. of Chicago Press, Chicago, 1968), p. 167.
18. S. J. Kenyon and L. Hartmann, *Astrophys. J. Suppl. Ser.* **101**, 117 (1995).
19. P. Kervella and P. Fouqué, *Astron. Astrophys.* **491**, 855 (2008).
20. R. Kohler and C. Leinert, *Astron. Astrophys.* **331**, 977 (1998).
21. E. L. Martin, in *Cool Stars in Clusters and Associations: Magnetic Activity and Age Indicators*, Ed. by G. Micela, R. Pallavicini, and S. Sciortino, *Mem. Soc. Astr. It.* **68**, 905 (1997).
22. E. L. Martin and A. Magazzù, *Astron. Astrophys.* **342**, 173 (1999).
23. A. Massarotti, D.W. Latham, G. Torres, et al., *Astron. J.* **129**, 2294 (2005).
24. A. F. L. Nemeç and J. M. Nemeç, *Astron. J.* **90**, 2317 (1985).
25. D. C. Nguyen, R. Jayawardhana, M.H. van Kerkwijk, et al., *Astrophysics* **695**, 1648 (2009).
26. P. Sartoretti, R. A. Brown, D. W. Latham, et al., *Astron. Astrophys.* **334**, 592 (1998).
27. L. Siess, E. Dufour, and M. Forestini, *Astron. Astrophys.* **358**, 593 (2000).
28. R.W. Tanner, *JRASC* **42**, 177 (1948).
29. A. Tokunaga, *Allen's Astrophysical Quantities*, 4th ed., Ed. by A. N. Cox (Springer, New York, 2000), p. 143.
30. G. Torres, J. Andersen, and A. Giménez, *Astron. Astrophys. Rev.* **18**, 67 (2010).
31. R. Wichmann, J. Krautter, J.H.M.M. Schmitt, et al., *Astron. Astrophys.* **312**, 439 (1996).
32. R. Wichmann, G. Torres, C. H. F. Melo, et al., *Astron. Astrophys.* **359**, 181 (2000).
33. Li-Feng Xing, Xiao-Bin Zhang, and Jian-Yan Wei, *Chin. J. Astron. Astrophys.* **6**, 716 (2006).